I&EC research
Industrial & Engineering Chemistry Research

Article

Cite This: Ind. Eng. Chem. Res. 2019, 58, 17399−17405

pubs.acs.org/IECR

Needleless Electrospinning for High Throughput Production of $Li_7La_3Zr_2O_{12}$ Solid Electrolyte Nanofibers

Tanner Rosenthal,[†] J. Mark Weller,[‡] and Candace K. Chan*[,‡]

[†]Electrical Engineering, School of Electrical, Computer and Energy Engineering and [‡]Materials Science and Engineering, School for Engineering of Matter, Transport and Energy, Arizona State University, 501 E Tyler Mall, ECG 301, Tempe, Arizona 85287, United States

Supporting Information

ABSTRACT: $Li_7La_3Zr_2O_{12}$ (LLZO) is a promising ceramic Li-ion conductor that has been successfully prepared in nanowire morphology using electrospinning from polymer/sol−gel solutions followed by calcination. However, conventional single-needle electrospinning has low production rates <0.1 g/h, making scale-up of the materials for applications in solid-state electrolytes challenging. Herein, needleless electrospinning using a twisted wire spinneret is employed to prepare Al-doped LLZO (ALLZO). We find that the appropriate precursor solutions for needleless electrospinning require much lower viscosity and are more sensitive to environmental conditions than those used in single-needle electrospinning. The as-formed nanofibers display a nanoribbon morphology, and calcination at 700 °C for 2 h in air results in phase pure ALLZO interconnected nanostructures with a cubic crystal structure. The results show that needleless electrospinning is an effective approach for preparing as-spun nanofibers with yields of ∼1 g/h possible, providing a higher throughput route toward Li^+ conducting nanostructures for solid-state battery applications.

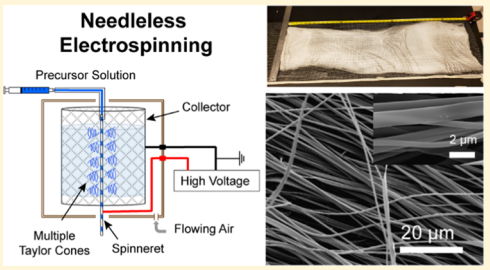

1. INTRODUCTION

Electrospinning is a versatile technique for preparing various ceramic nanofibers from sol−gel precursors.[1−3] In a typical lab-scale electrospinning setup, a high voltage power supply is used to apply a large bias between a spinneret consisting of a syringe needle and a flat metal collector, while a syringe pump pushes the precursor solution through the spinneret tip to form electrified droplets.[2] This solution typically contains the sol−gel precursors for the ceramic material of interest mixed with a polymer. A cone (known as a Taylor cone) forms on the tip from which a polymer jet is ejected and forms a continuous fiber that is deposited onto the collector as a mat. The nanofiber mat can then be recovered from the collector and calcined to remove the organic components and crystallize the sol−gel precursor, resulting in ceramic nanofibers. Although widely used for the preparation of a broad range of nanofibers, one drawback of conventional single-needle electrospinning (SNE) is its low material production rates (0.01−0.1 g/h).[4]

Ceramic nanofibers prepared by electrospinning have attracted much interest recently for use in batteries, owing to the advantages imparted by the one-dimensional morphology, such as large surface-to-volume ratio, short ionic transport lengths, and efficient electron transport along the nanofiber diameter and longitudinal directions.[5] Lithium-ion battery electrodes comprising electrospun nanofibers of $LiCoO_2$,[6] $LiMn_2O_4$,[7] $Li_{1.2}Ni_{0.17}Co_{0.17}Mn_{0.5}O_2$,[8] and $Li_4Ti_5O_{12}$[9,10] have been reported with improved specific capacity and enhanced rate performance compared to conventional particulate active materials. The electrospinning of Li-ion conducting ceramics has also received great interest recently,[11] with $Li_{0.33}La_{0.557}TiO_3$,[12−14] $Li_{1.3}Al_{0.3}Ti_{1.7}(PO_4)_3$,[15] and $Li_7La_3Zr_2O_{12}$ (LLZO)[16,17] nanofibers showing promise as solid-state electrolytes in densified ceramics and polymer composites. In particular, solid polymer electrolytes containing electrospun LLZO nanofibers as ceramic fillers have improved cycle life (up to 1000 h of cycling)[16] due to the suppression of lithium dendrite growth and 2−3 orders of higher ionic conductivity compared to the polymers alone.[16−18]

In our previous work, we demonstrated that polycrystalline nanowires of LLZO could be successfully prepared using a conventional lab-scale, single-needle electrospinning setup from aqueous sol−gel solutions,[19] which was later extended to nonaqueous precursor solutions.[16,17] However, the mass of the LLZO nanowires recovered after calcination is typically about one-fourth the mass of the as-spun nanofibers when using precursors with the aqueous solvent (or one-seventh when using the nonaqueous solvent).[20] With a typical production rate of 0.08−0.1 g/h using single-needle electrospinning, very long spinning times are required to obtain enough materials to characterize the properties of LLZO nanofibers for solid-state electrolyte applications and to utilize these materials in all-solid-state batteries.

Received: June 20, 2019
Revised: August 21, 2019
Accepted: August 26, 2019
Published: August 26, 2019

DOI: 10.1021/acs.iecr.9b03376
Ind. Eng. Chem. Res. 2019, 58, 17399−17405

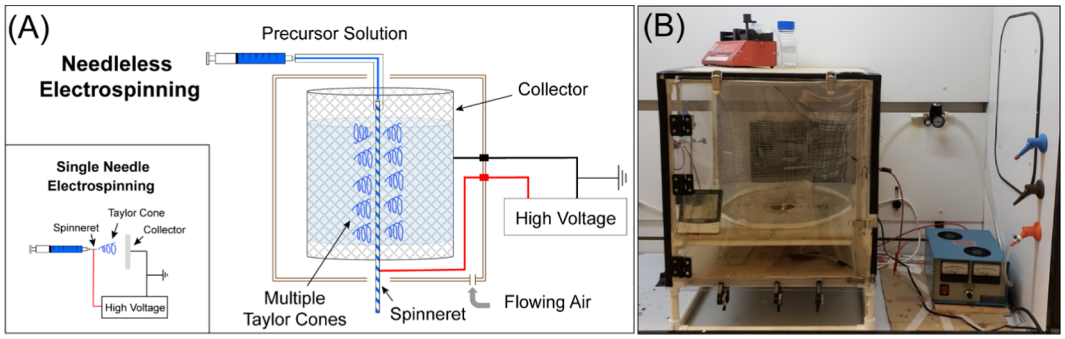

Figure 1. (A) Schematic of needleless electrospinning reactor built based on the design reported by Holopainen et al.;[28] the inset shows a schematic of conventional single-needle electrospinning for comparison. (B) Photograph of the needleless electrospinning reactor.

Electrospinning approaches such as those that use multiple needles[21−23] or rotating cylinders[24,25] as spinnerets have attracted much interest for their potential to greatly improve nanofiber production rates. Needleless electrospinning, wherein multiple polymer jets are formed from an open liquid surface, are particularly attractive for increasing throughput.[4,26,27] A simple needleless electrospinning approach reported by Holopainen et al.[28] used a twisted wire as a spinneret to prepare nanofibers of poly(vinylpyrrolidone) (PVP) and hydroxyapatite. In this method, the twisted metal wire is vertically oriented in the center of a stationary cylindrical collector made of metallic mesh; the precursor solution is fed from the top of the wire and flows down the length of the wire assisted by gravity. Meanwhile, nanofibers are formed from multiple Taylor cones along the length of the twisted wire, resulting in deposition of the nanofiber mat on the inner surface of the cylinder. Using twisted wire electrospinning, mats of PVP nanofibers 40 × 120 cm^2 were prepared with a production rate as high as 5.23 g/h. For the hydroxyapatite nanofibers, it was not possible to use as high of a precursor concentration in the electrospinning solution as is typically used in conventional single-needle electrospinning, but the production rates were nevertheless increased 15-fold from 0.09 to 1.4 g/h. These results show that needleless electrospinning based on a twisted wire spinneret could be a promising approach for the large-scale production of ceramic nanofibers.

Herein, we report the synthesis of Al-doped LLZO (ALLZO) nanofibers via needleless electrospinning for the first time, using a twisted wire spinneret reactor based on that reported by Holopainen et al.[28] Due to the different reactor geometries, the LLZO nonaqueous precursor solutions developed for single-needle electrospinning were reoptimized for needleless electrospinning. The effect of precursor solution properties and electrospinning parameters on the morphology of the as-spun nanofibers was studied. The calcination conditions needed to form ALLZO from the nanofibers were also studied, along with detailed structural characterization to assess the phase purity and dopant distribution. The results show that needleless electrospinning is an effective approach for preparing as-spun nanofibers with nanoribbon morphology and yields of ∼1 g/h possible. Suitable precursor solutions for needleless electrospinning require much lower viscosity than those used in single-needle electrospinning. Calcination of the electrospun fibers at 700 °C for 2 h in air was sufficient to form phase pure ALLZO interconnected nanostructures with ligament morphology and cubic crystal structure, although long exposure of as-spun nanofibers to ambient atmosphere prior to calcination caused the formation of secondary phases. The results demonstrate that needleless electrospinning could be a simple and practical way to scale-up the production of ALLZO nanostructures from electrospun nanofibers.

2. EXPERIMENTAL METHODS

2.1. LLZO Precursor Preparation. The LLZO sol−gel was prepared from $LiNO_3$, zirconium(IV) *n*-propoxide, $La(NO_3)_3{\cdot}6H_2O$, and $Al(NO_3)_3{\cdot}9H_2O$. Al^{3+} doping was used to stabilize the highly conducting cubic phase of LLZO.[29,30] The Li, La, and Al precursors were dissolved in a solution mixture comprised of ethanol, *N*,*N*-dimethylformamide (DMF), and deionized water. The Zr precursor was separately dissolved in glacial acetic acid. Then, the two precursor solutions were mixed thoroughly, and poly(vinylpyrrolidone) (PVP) was added after all of the precursors had dissolved. The precursor solutions were stable and could be used over the course of several weeks without any issues. More details about the amounts and specifications of the chemical reagents are provided in the Supporting Information.

2.2. Electrospinning Reactor. The needleless electrospinning reactor was built based on the design reported by Holopainen et al.[28] using a twisted wire as the spinneret and wire mesh as the collector. Photographs of the reactor are shown in Figure 1, with a more detailed description in the Supporting Information and additional photographs of the components shown in Figure S1. House-compressed air at 5 psi was fed into the chamber continuously during the electrospinning to control the humidity, which was kept between 12 and 15% relative humidity, while the laboratory temperature was maintained at 20−22 °C. In each experiment, the voltage between the spinneret and collector was kept at 20 kV, and the precursor solution was fed at a rate of 15 mL/h.

2.3. Materials Characterization. Powder X-ray diffraction (XRD) was performed using a Bruker D8 powder X-ray diffractometer with Cu Kα radiation from 15° < 2θ < 60° at 0.02° increments. The morphology of the as-spun and calcined nanofibers was assessed using an XL30 environmental FEG-FEI scanning electron microscopy (SEM). The samples were sputter-coated with a thin layer of Au−Pd to minimize charging. Nanofiber diameters were measured using ImageJ. Scanning transmission electron microscopy (STEM) and energy-dispersive X-ray spectroscopy (EDS) were performed on a JEOL ARM200 probe-corrected microscope equipped with a windowless JEOL EDS spectrometer. EDS data and maps were processed using the open-source Cornell Spectrum Imager[31] plugin in ImageJ. Thermogravimetric analysis (TGA) was carried out using a Labsys Evo (Setaram) in the air from

DOI: 10.1021/acs.iecr.9b03376
Ind. Eng. Chem. Res. 2019, 58, 17399−17405

room temperature to 900 °C with a heating rate of 5 °C/min. Viscosity measurements were obtained using an AR-G2 Rheometer (TA Instruments) at 25 °C using a 25 mm steel parallel plate geometry, 50 micrometer gap during testing, strain sweep testing mode, and angular frequency of 6.28319 rad/s (1 Hz).

2.4. Calcination. The as-spun nanofibers were calcined in a box furnace (Carbolite ELF 11/14B) or tube furnace (Lindberg Blue M) in air using a 5 °C/min ramp rate and hold at 700 °C for various times between 0.5 and 3 h, followed by natural cooling to room temperature. For calcination in the box furnace, the entire piece of the as-spun nanofiber mat (approximately 41 × 12 $in.^2$) was placed vertically inside a 250 mL volume alumina crucible (CoorsTek). For calcination in the tube furnace, approximately half of the as-spun mat was folded and placed in an alumina combustion boat (CoorsTek).

3. RESULTS AND DISCUSSION

3.1. Electrospinning Precursor Solutions and Parameters. Figure 1 shows a photograph and schematic of the needleless electrospinning reactor, with a conventional single-needle electrospinning (from now on, abbreviated as SNE) schematic shown in the inset of Figure 1A. The details for the synthesis of LLZO nanowires in a conventional setup using a syringe needle as the spinneret and the flat aluminum foil collector were described in our previous work.[17,19,20]

In a typical SNE experiment, the voltage used was between 7 and 11 kV, the distance between the needle tip and the collector was between 10 and 15 cm, and the precursor solution was fed through the syringe at a rate of 0.1−0.3 mL/h. Both aqueous and nonaqueous sol−gel precursors were used; however, the nonaqueous precursor resulted in nanofibers that required shorter calcination times to form LLZO and the resulting calcined nanowires had improved morphology compared to those prepared from the aqueous precursor.[17,20] In both cases, the LLZO sol−gel solution was mixed with a solution of 15 wt % PVP in acetic acid (used to stabilize the sol−gel precursors and prevent premature hydrolysis)[1,32] at a 2:1 volume ratio (for aqueous solutions) or 1:1 volume ratio (for the nonaqueous solution). A typical nanofiber production rate was 0.08−0.1 g/h. In the work by Holopainen et al., electrospinning precursor solutions of identical composition and viscosity (around 0.2 Pa s) could be used on both needleless and SNE reactors for preparing PVP nanofibers.[28] However, we found that the viscosity of the optimized SNE precursor solution for LLZO was too high (>12 Pa s) for use in the needleless reactor. The viscosity of the solution is important since the precursor must travel down the length of the spinneret, with the twist in the wire enabling the precursor to rotate such that Taylor cones are formed radially over all 360°, depositing nanofibers onto the inner surface of the collector, as depicted in Figure 1A. To decrease the viscosity, a mixture of water and ethanol was added to dissolve the Li, La, and Al precursors, instead of just using DMF and acetic acid as in the SNE precursor. Table 1 summarizes the wt % of components for the optimized solution mixture (actual amounts of reagents are described in the Supporting Information), compared to the SNE precursor, along with the measured viscosities for both solutions.

Along with the different solvent composition, the wt % of PVP in the needleless solution had to be increased to exceed the percentage of LLZO precursors, whereas the loading of precursor reagents was higher in the SNE solution. Using the solution optimized for the needleless reactor (viscosity of 0.17 Pa s), 0.23 g/h of as-spun nanofibers could be obtained using a precursor feed rate of 10 mL/h and applied voltage bias of 15 kV between the spinneret and collector. This production rate was increased by increasing the feed rate to 15 mL/h and voltage to 20 kV, with an average rate of 1.023 ± 0.094 g/h over 14 reactions with good reproducibility (Table S1). Compared to a typical nanofiber production rate using SNE, the needleless electrospinning offers a higher production rate by approximately 1 order of magnitude. One disadvantage of the needleless reactor, as first observed by Holopainen et al.,[28] is the gelling or drying of the solution on the twisted wire, which requires cleaning in between use and limits prolonged synthesis. Typically, needleless electrospinning could be performed continuously for 45 min at a time to produce, on average, 767 mg of nanofibers, before needing to be stopped and cleaned. However, this gelling process, which occurs due to solvent evaporation, is analogous to clogging of the needle in conventional electrospinning,[33,34] which similarly limits SNE of LLZO to ∼2 h of synthesis time before the needle needs to be cleaned.

Table 1. Comparison of LLZO Single-Needle Electrospinning and Needleless Electrospinning Precursors (wt % are Reported with Respect to the Total Mass after Combining the Li/La/Al- and Zr-Containing Solutions)

	single needle	needleless
acetic acid/DMF/H_2O/EtOH (by vol.)	1.4:1:0:0	1:25:12.5:75
wt % LLZO precursors	8.32	2.29
wt % PVP	6.60	7.49
wt % solvent	85.08	90.22
PVP/precursors (by wt)	0.79:1	3.27:1
viscosity (Pa s)	12.34	0.17

Figure 2A shows a photograph of a nanofiber mat prepared after 45 min of needleless electrospinning reaction (approximate dimensions: 41 × 10 $in.^2$). The deposition of nanofibers on the mat was very uniform, confirming the radial formation of liquid jets from the spinneret. The mat could be easily removed from the collector as a single piece (the lower left-hand corner of the mat in Figure 2A is partially removed). Scanning electron microscopy (SEM) imaging showed that the as-spun nanofibers exhibited a nanoribbon morphology with more of a rectangular cross-section (Figure 2B), with the average diameter/width of 650 nm (Figure 2C). The morphology of the as-spun nanofibers was consistent throughout the mat, except some curled fibers were observed close to the edges of the mat (Figure S2), likely due to nonuniform electric field distribution at either end of the collector. The nanoribbon morphology in materials produced with needleless electrospinning is different from what was observed in as-spun nanofibers prepared using SNE, which had cylindrical cross-sections. Similar morphologies have been observed previously and have been attributed to the formation of a thin polymer skin on the surface of the liquid jet that collapses into a flat nanoribbon due to solvent evaporation.[35] In our case, this is a feasible explanation as well, since the needleless electrospinning precursor required a large vol % of ethanol; the ribbon morphology may also be a feature of this type of reactor, as Holopainen et al. also reported similar morphologies for PVP and hydroxyapatite nanofibers produced in their setup.[28]

DOI: 10.1021/acs.iecr.9b03376
Ind. Eng. Chem. Res. 2019, 58, 17399−17405

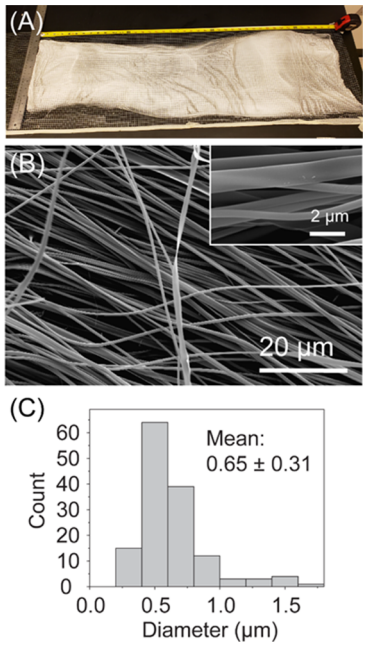

Figure 2. (A) Photograph of the LLZO nanofiber mat prepared using needleless electrospinning, (B) SEM (the inset shows a magnified view showing nanoribbon morphology), and (C) diameter distribution of as-spun nanofibers with mean ± standard deviation in the inset (units: microns).

3.2. Calcination Studies. To better understand the thermal decomposition behavior of the as-spun nanofibers, thermogravimetric analysis (TGA) was performed. For comparison, TGA was also performed on the precursor solution that was dried at 50 °C to remove all of the solvents as well as on pristine PVP powder. Due to the agglomeration of the particles comprising the dried precursor and as-obtained PVP powder, the TGA results show less complete combustion (i.e., higher residual mass) for these samples compared to the nonagglomerated nanofibers. As shown in Figure 3A, the weight loss curves for the nanofibers and precursor at low temperatures resembled that for PVP, with thermal degradation of the polymer beginning at around 240 °C and increasing above 400 °C, similar to previous reports.[36,37] The weight loss between 400 and 600 °C is hence attributed to the decomposition of the LLZO sol−gel precursors, consistent with the reported decomposition temperatures for lithium nitrate (~500 °C)[38] and lanthanum nitrate (from ~320 to 610 °C).[39,40] Some of the weight loss between 215 and 400 °C could be from the decomposition of zirconium propoxide based on prior observations.[41] No further weight loss was observed above 650 °C for the as-spun nanofibers, indicating that the organic components were completely removed. Therefore, to crystallize the sol−gel precursors to form LLZO, the as-spun nanofibers were calcined in air at 700 °C for various times. Typically, only about 8% of the original as-spun nanofiber mass was retained after calcination, but the mass of crystallized LLZO obtained per hour of synthesis was still more than 5 times higher than that obtained from SNE due to the higher production rates of the electrospinning (Table S2).

As shown in Figure 3B, the XRD patterns showed that the cubic phase of ALLZO could be formed after only using a 0.5 h hold at 700 °C. However, broad reflections associated with the (222), (004), (044), and (225) planes for $La_2Zr_2O_7$ with

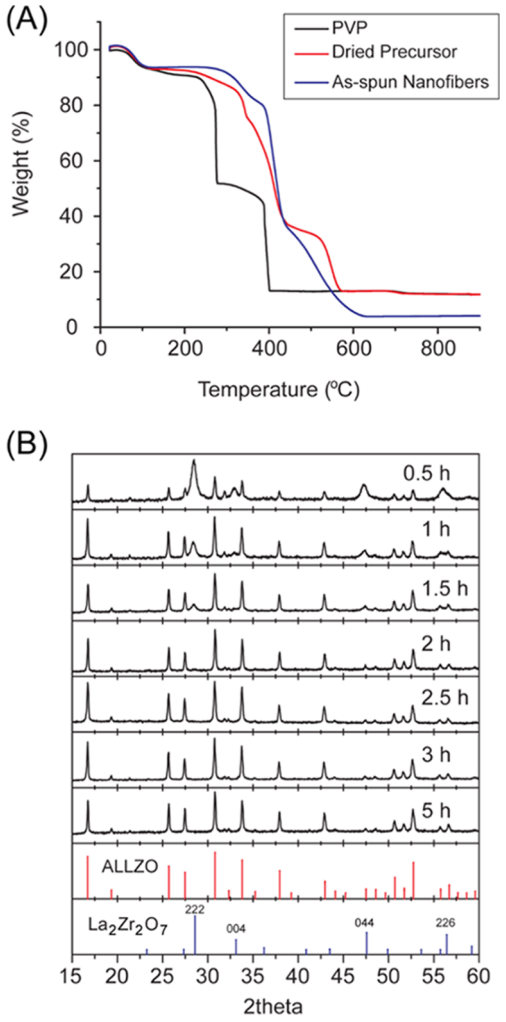

Figure 3. (A) TGA results obtained by heating as-spun nanofibers, dried electrospinning precursor, and the PVP powder in the air; (B) XRD patterns of nanofibers after calcination at 700 °C for different times in the box furnace, compared with reference patterns for $Li_{6.06}Al_{0.20}La_3Zr_2O_{12}$ (from the structure reported by Buschmann et al.[29]) and $La_2Zr_2O_7$ (from Harvey et al.[42]).

pyrochlore structure were also observed and remained visible until a calcination time of 2 h was used. $La_2Zr_2O_7$ is a known intermediate phase in the synthesis of LLZO and was observed in the SNE synthesis of LLZO as well; its presence indicates that further calcination is needed so that $La_2Zr_2O_7$ can completely react to LLZO (presumably with amorphous phases containing the rest of the Li and La needed).[19] However, our previous study showed that phase pure LLZO could be obtained after calcination at 700 °C for 1 h.[17] The longer calcination times required here could be due to the different solvent compositions used in the precursor solution for needleless electrospinning.

SEM imaging was performed to understand the diameter and morphology evolution of the ALLZO nanofibers after different calcination times. The manner in which the as-spun nanofiber mats were calcined was found to have an effect on the resulting morphology. When rolling the mats up and placing them inside a combustion boat in a tube furnace, the materials lost their wire shape and displayed an interconnected ligament structure with "coral-like" morphology after calcination (Figure S3). This may have occurred because the

DOI: 10.1021/acs.iecr.9b03376
Ind. Eng. Chem. Res. 2019, 58, 17399−17405

nanofibers were compacted together in the boat, making coalescence more likely to occur during heating or from enhanced local heating and combustion rates in the tightly packed fibers. To mitigate these effects, the as-spun nanofiber mats were loosely crumpled into a ball and placed inside a large crucible (Figure S4) and calcined inside a box furnace. After calcination, the mat maintained its overall shape but with a reduced volume due to the large mass loss from removal of organic and precursor species.

The nanowires calcined for 1 h in the crucible still displayed ribbon morphologies similar to those seen in the as-spun nanofibers, but pores could be clearly observed, particularly near the centers of the nanoribbons (Figure 4A, the inset shows a higher magnification view). The porosity made the morphology somewhat fragile, as grinding the calcined powder with a mortar and pestle was sufficient to destroy some of the nanoribbons, leaving nanowire-like morphologies that appear to originate from the former edges of the nanoribbons (Figure 4B). The SEM images of the nanofibers calcined for 3 h showed that the morphology further changed to the interconnected coral-like structure, which is similar to what we have observed in previous studies[19] (Figure 4C). After 5 h of calcination, the morphology of the sample resembled an interconnected nanowire network (Figure 4D), which may have formed due to coalescence of the ligament structures observed in Figure 4C. The analysis of the diameter distribution of the calcined samples (Figure 4E) showed that the nanofibers calcined for 1 h had an average width of ∼590 nm, slightly smaller than the average widths of the as-spun fibers (∼650 nm). The average diameter and diameter distribution decreased substantially after calcination at 3 h, with most of the ligaments around 200 nm in width. The sample calcined for 5 h had slightly higher average diameter of ∼320 nm, which is consistent with the coalescence of the ALLZO ligaments with prolonged heating.

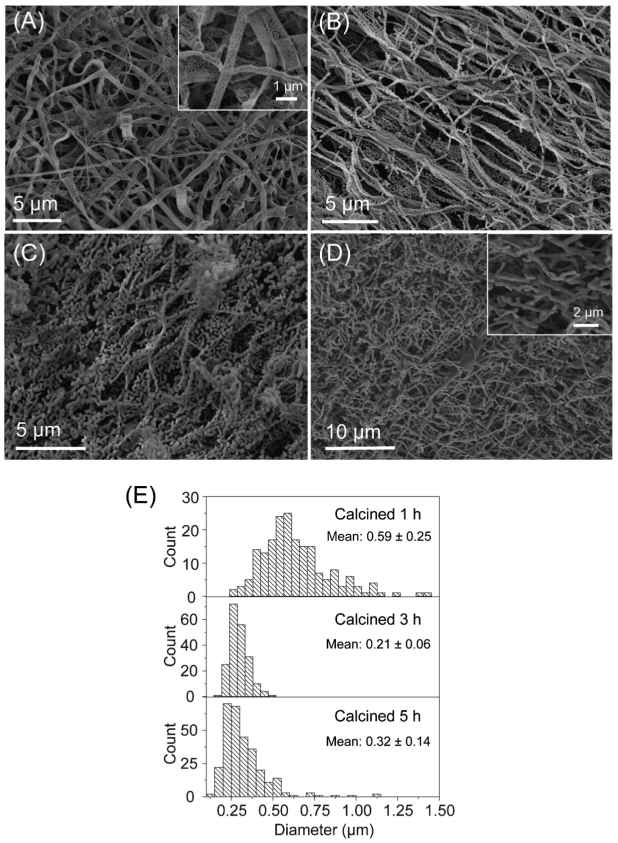

Figure 4. SEM images of ALLZO prepared using needleless electrospinning after calcination at 700 °C for (A) 1 h, (B) 1 h after grinding, (C) 3 h, (D) 5 h; and (E) diameter distribution of ALLZO calcined for 1, 3, and 5 h (no grinding). The mean diameter/width ± sample standard deviation (units: microns) are indicated in the inset.

To check the composition and dopant uniformity, high-angle annular dark-field (HAADF) scanning transmission electron microscopy (STEM) was performed on the ALLZO nanowires obtained after calcination at 2 h. Energy-dispersive X-ray spectroscopy (EDS) spectral images were acquired simultaneously of the area enclosed by the red box in the HAADF-STEM image in Figure 5. As seen by EDS maps, the La, Zr, and Al signals were uniformly distributed across the materials, demonstrating good dispersion of the Al^{3+} dopant within the LLZO.

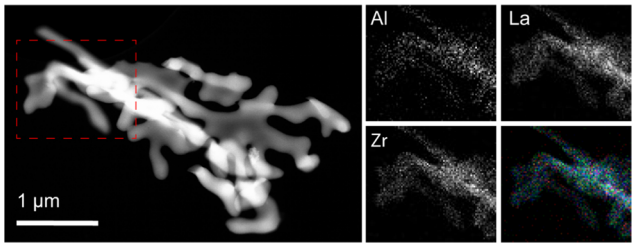

Figure 5. Survey HAADF-STEM image of ALLZO after 2 h calcination with the region of interest enclosed by the red box with corresponding STEM-EDS maps (in the combined image, Al = red, La = blue, Zr = green).

It should be noted that the phase purity of the LLZO nanofibers prepared using needleless electrospinning was found to be sensitive to the environmental and sample storage conditions. The precursor used to prepare LLZO via SNE was not susceptible to hydrolysis in the ambient conditions of our laboratory (keeping in mind that in the desert environment of Arizona, relative humidity levels are typically between 20 and 50%),[43] and the SNE reactor did not need to be contained inside a humidity-controlled enclosure. On the other hand, initial attempts to perform needleless electrospinning in the ambient atmosphere were not successful, and an enclosure with a constant air flow to maintain relative humidity below 17% was needed. If the relative humidity exceeded ∼25%, electrospraying of droplets would occur. This increased sensitivity to hydrolysis can be explained by the inclusion of 12.5 wt % water to the precursor solution to obtain the viscosity needed for the fiber production using the needleless reactor. The phase purity of the calcined LLZO was also found to be sensitive to the ambient environment if the as-spun nanofibers were stored in the laboratory prior to heat treatment, perhaps due to hydrolysis of the sol−gel precursors. The XRD patterns of samples that had been stored for 4−10 days in ambient conditions prior to calcination show strong reflections from $La_2Li_{0.5}Al_{0.5}O_4$[44] as an impurity phase, which were still visible in samples calcined for longer times (Figure S5A). These results implied that the reaction of the sol−gel precursors and/or ageing may have occurred during the period between the sample preparation and the calcination, which had a detrimental effect on the phase purity of the calcined

DOI: 10.1021/acs.iecr.9b03376
Ind. Eng. Chem. Res. 2019, 58, 17399−17405

samples. Notably, $La_2Zr_2O_7$ was not observed as an intermediate phase for calcination times below 2 h, different for freshly calcined nanofibers (Figure 3), while the LLZO formed still adopted the cubic phase. This implies that although the $La_2Li_{0.5}Al_{0.5}O_4$ acted as an irreversible lanthanum "sink" to prevent the formation of $La_2Zr_2O_7$ (which, in contrast, can react further to form LLZO), it did not prevent the stabilization of the cubic phase of LLZO even though it presumably would have utilized all of the Al^{3+} dopants to form this compound. The LLZO likely displayed the cubic phase and not the tetragonal one as a result of the small feature sizes of the calcined nanowires, as the formation of cubic LLZO in undoped nanostructures has been reported before and likely arises as a size-stabilization effect.[19,45,46] Therefore, to preserve phase purity, the as-spun nanofibers were either calcined immediately after electrospinning or stored in an Ar-filled glovebox to prevent hydrolysis until calcination. We found that phase pure ALLZO could be obtained even after storing as-spun nanofibers long term (e.g., 19 days) inside the glovebox (Figure S5B), indicating the stability of the materials in the absence of air/water.

4. CONCLUSIONS

In summary, we have shown that needleless electrospinning can be used to increase the throughput of LLZO precursor nanofibers by an order of magnitude, with production rates of ~1 g/h possible. The precursor solution optimized to prepare LLZO via single-needle electrospinning is unsuitable for needleless electrospinning. We find that the wt % of PVP must be increased, while the wt % of LLZO precursors and solution viscosity must be greatly decreased, in part by adding water and ethanol to the solvent mixture. The increased sensitivity of the needleless electrospinning process can be mitigated by controlling the relative humidity of the reactor environment and preventing the nanofiber mats from undergoing hydrolysis prior to calcination. The as-spun nanofibers display a nanoribbon morphology, which is partially retained in the calcined materials. Calcination at 700 °C for 2 h was sufficient to form cubic phase LLZO with uniform Al^{3+} dopant distribution. These results show that needleless electrospinning is effective for higher throughput synthesis of LLZO materials, which can facilitate the mass production of solid-state electrolytes for next-generation Li batteries.

■ ASSOCIATED CONTENT

Supporting Information

The Supporting Information is available free of charge on the ACS Publications website at DOI: 10.1021/acs.iecr.9b03376.

Experimental procedures for synthesis; detailed description of the needleless electrospinning reactor; production statistics for needleless electrospinning; photographs of reactor and components; additional XRD patterns and SEM images (PDF)

■ AUTHOR INFORMATION

Corresponding Author

*E-mail: candace.chan@asu.edu.

ORCID

J. Mark Weller: 0000-0003-2056-8974

Candace K. Chan: 0000-0003-4329-4865

Author Contributions

The manuscript was written through contributions of all of the authors. All of the authors have given approval to the final version of the manuscript.

Notes

The authors declare no competing financial interest.

■ ACKNOWLEDGMENTS

This work was supported by the NSF CAREER award DMR 1553519 with partial support from the NSF Nanosystems Engineering Research Center for Nanotechnology Enabled Water Treatment (EEC-1449500). The authors gratefully acknowledge the use of facilities within the Eyring Materials Center and John M. Cowley Center for High Resolution Electron Microscopy at Arizona State University. J.M.W. acknowledges the support from an ASU Fulton Schools of Engineering Dean's Fellowship. We are grateful to Y. Xu and L. Dai for assistance with the viscosity measurements.

■ REFERENCES

(1) Li, D.; Xia, Y. Fabrication of Titania Nanofibers by Electrospinning. *Nano Lett.* **2003**, *3*, 555−560.

(2) Li, D.; McCann, J. T.; Xia, Y.; Marquez, M. Electrospinning: A Simple and Versatile Technique for Producing Ceramic Nanofibers and Nanotubes. *J. Am. Ceram. Soc.* **2006**, *89*, 1861.

(3) Ramaseshan, R.; Sundarrajan, S.; Jose, R.; Ramakrishna, S. Nanostructured Ceramics by Electrospinning. *J. Appl. Phys.* **2007**, *102*, No. 111101.

(4) Yu, M.; Dong, R. H.; Yan, X.; Yu, G. F.; You, M. H.; Ning, X.; Long, Y. Z. Recent Advances in Needleless Electrospinning of Ultrathin Fibers: From Academia to Industrial Production. *Macromol. Mater. Eng.* **2017**, *302*, No. 1700002.

(5) Wang, H. G.; Yuan, S.; Ma, D. L.; Zhang, X. B.; Yan, J. M. Electrospun Materials for Lithium and Sodium Rechargeable Batteries: From Structure Evolution to Electrochemical Performance. *Energy Environ. Sci.* **2015**, *8*, 1660.

(6) Gu, Y.; Chen, D.; Jiao, X. Synthesis and Electrochemical Properties of Nanostructured $LiCoO_2$ Fibers as Cathode Materials for Lithium-Ion Batteries. *J. Phys. Chem. B* **2005**, *109*, 17901.

(7) Aravindan, V.; Sundaramurthy, J.; Kumar, P. S.; Shubha, N.; Ling, W. C.; Ramakrishna, S.; Madhavi, S. A Novel Strategy to Construct High Performance Lithium-Ion Cells Using One Dimensional Electrospun Nanofibers, Electrodes and Separators. *Nanoscale* **2013**, *5*, 10636.

(8) Min, J. W.; Yim, C. J.; Im, W. B. Facile Synthesis of Electrospun $Li_{1.2}Ni_{0.17}Co_{0.17}Mn_{0.5}O_2$ Nanofiber and Its Enhanced High-Rate Performance for Lithium-Ion Battery Applications. *ACS Appl. Mater. Interfaces* **2013**, *5*, 7765.

(9) Jo, M. R.; Jung, Y. S.; Kang, Y. M. Tailored $Li_4Ti_5O_{12}$ Nanofibers with Outstanding Kinetics for Lithium Rechargeable Batteries. *Nanoscale* **2012**, *4*, 6870.

(10) Guo, B.; Li, Y.; Yao, Y.; Lin, Z.; Ji, L.; Xu, G.; Liang, Y.; Shi, Q.; Zhang, X. Electrospun $Li_4Ti_5O_{12}$/C Composites for Lithium-Ion Batteries with High Rate Performance. *Solid State Ionics* **2011**, *204−205*, 61.

(11) La Monaca, A.; Paolella, A.; Guerfi, A.; Rosei, F.; Zaghib, K. Electrospun Ceramic Nanofibers as 1D Solid Electrolytes for Lithium Batteries. *Electrochem. Commun.* **2019**, *104*, No. 106483.

(12) Yang, T.; Li, Y.; Chan, C. K. Enhanced Lithium Ion Conductivity in Lithium Lanthanum Titanate Solid Electrolyte Nanowires Prepared by Electrospinning. *J. Power Sources* **2015**, *287*, 164.

(13) Liu, W.; Liu, N.; Sun, J.; Hsu, P.-C.; Li, Y.; Lee, H.-W.; Cui, Y. Ionic Conductivity Enhancement of Polymer Electrolytes with Ceramic Nanowire Fillers. *Nano Lett.* **2015**, *15*, 2740.

(14) Liu, W.; Lee, S. W.; Lin, D.; Shi, F.; Wang, S.; Sendek, A. D.; Cui, Y. Enhancing Ionic Conductivity in Composite Polymer

Electrolytes with Well-Aligned Ceramic Nanowires. *Nat. Energy* **2017**, *2*, No. 17035.
(15) Lancel, G.; Stevens, P.; Toussaint, G.; Maréchal, M.; Krins, N.; Bregiroux, D.; Laberty-Robert, C. Hybrid Li Ion Conducting Membrane as Protection for the Li Anode in an Aqueous Li-Air Battery: Coupling Sol-Gel Chemistry and Electrospinning. *Langmuir* **2017**, *33*, 9288.
(16) Fu, K.; Gong, Y.; Dai, J.; Gong, A.; Han, X.; Yao, Y.; Wang, C.; Wang, Y.; Chen, Y.; Yan, C.; et al. Flexible, Solid-State, Ion-Conducting Membrane with 3D Garnet Nanofiber Networks for Lithium Batteries. *Proc. Natl. Acad. Sci. U.S.A.* **2016**, *113*, 7094.
(17) Yang, T.; Zheng, J.; Cheng, Q.; Hu, Y. Y.; Chan, C. K. Composite Polymer Electrolytes with $Li_7La_3Zr_2O_{12}$ Garnet-Type Nanowires as Ceramic Fillers: Mechanism of Conductivity Enhancement and Role of Doping and Morphology. *ACS Appl. Mater. Interfaces* **2017**, *9*, 21773.
(18) Wan, Z.; Lei, D.; Yang, W.; Liu, C.; Shi, K.; Hao, X.; Shen, L.; Lv, W. Low Resistance − Integrated All-Solid-State Battery Achieved by $Li_7La_3Zr_2O_{12}$ Nanowire Upgrading Polyethylene Oxide (PEO) Composite Electrolyte and PEO Cathode Binder. *Adv. Funct. Mater.* **2019**, *1805301*, 1.
(19) Yang, T.; Gordon, Z. D.; Li, Y.; Chan, C. K. Nanostructured Garnet-Type Solid Electrolytes for Lithium Batteries: Electrospinning Synthesis of $Li_7La_3Zr_2O_{12}$ Nanowires and Particle Size-Dependent Phase Transformation. *J. Phys. Chem. C* **2015**, *119*, 14947.
(20) Chan, C. K.; Yang, T.; Mark Weller, J. Nanostructured Garnet-Type $Li_7La_3Zr_2O_{12}$: Synthesis, Properties, and Opportunities as Electrolytes for Li-Ion Batteries. *Electrochim. Acta* **2017**, *253*, 268.
(21) Ding, B.; Kimura, E.; Sato, T.; Fujita, S.; Shiratori, S. Fabrication of Blend Biodegradable Nanofibrous Nonwoven Mats via Multi-Jet Electrospinning. *Polymer* **2004**, *45*, 1895.
(22) Theron, S. A.; Yarin, A. L.; Zussman, E.; Kroll, E. Multiple Jets in Electrospinning: Experiment and Modeling. *Polymer* **2005**, *46*, 2889.
(23) Varesano, A.; Carletto, R. A.; Mazzuchetti, G. Experimental Investigations on the Multi-Jet Electrospinning Process. *J. Mater. Process. Technol.* **2009**, *209*, 5178.
(24) Jirsak, O.; Sanetrnik, F.; Lukas, D.; Kotek, V.; Martinova, L.; Chaloupek, J. Method of Nanofibres Production from a Polymer Solution Using Electrostatic Spinning and a Device for Carrying out the Method, 2009.
(25) Niu, H.; Lin, T.; Wang, X. Needleless Electrospinning. I. A Comparison of Cylinder and Disk Nozzles. *J. Appl. Polym. Sci.* **2009**, *114*, 3524.
(26) Niu, H.; Wang, X.; Lin, T. Needleless Electrospinning: Developments and Performances, In *Nanofibers - Production, Properties and Functional Applications*; Lin, T., Ed.; InTech Europe: Rijeka, 2011; pp 17−36.
(27) Lin, T. Needleless Electrospinning: A Practical Way to Mass Production of Nanofibers. *J. Text. Sci. Eng.* **2012**, *02*, 2.
(28) Holopainen, J.; Penttinen, T.; Santala, E.; Ritala, M. Needleless Electrospinning with Twisted Wire Spinneret. *Nanotechnology* **2015**, *26*, No. 025301.
(29) Buschmann, H.; Doïle, J.; Berendts, S.; Kuhn, A.; Bottke, P.; Wilkening, M.; Heitjans, P.; Senyshyn, A.; Ehrenberg, H.; Lotnyk, A.; et al. Structure and Dynamics of the Fast Lithium Ion Conductor "$Li_7La_3Zr_2O_{12}$.". *Phys. Chem. Chem. Phys.* **2011**, *13*, 19378.
(30) Rangasamy, E.; Wolfenstine, J.; Sakamoto, J. The Role of Al and Li Concentration on the Formation of Cubic Garnet Solid Electrolyte of Nominal Composition $Li_7La_3Zr_2O_{12}$. *Solid State Ionics* **2012**, *206*, 28.
(31) Hovden, R.; Cueva, P.; Mundy, J. A.; Muller, D. A. The Open-Source Cornell Spectrum Imager. *Micros. Today* **2013**, *21*, 40.
(32) Yi, G.; Sayer, M. An Acetic Acid/Water Based Sol-Gel PZT Process II: Formation of a Water Based Solution. *J. Sol-Gel Sci. Technol.* **1996**, *6*, 75.
(33) Kanjanapongkul, K.; Wongsasulak, S.; Yoovidhya, T. Investigation and Prevention of Clogging During Electrospinning of Zein Solution. *J. Appl. Polym. Sci.* **2010**, *118*, 1821.
(34) Kanjanapongkul, K.; Wongsasulak, S.; Yoovidhya, T. Prediction of Clogging Time during Electrospinning of Zein Solution: Scaling Analysis and Experimental Verification. *Chem. Eng. Sci.* **2010**, *65*, 5217.
(35) Koombhongse, S.; Liu, W.; Reneker, D. H. Flat Polymer Ribbons and Other Shapes by Electrospinning. *J. Polym. Sci., Part B: Polym. Phys.* **2001**, *39*, 2598.
(36) Rao, V.; Latha, P.; Ashokan, P. V.; Shridhar, M. H. Thermal Degradation of Poly(N-Vinylpyrrolidone)-Poly(Vinyl Alcohol) Blends. *Polym. J.* **1999**, *31*, 887.
(37) Kozuka, H.; Takenaka, S. Single-Step Deposition of Gel-Derived Lead Zirconate Titanate Films: Critical Thickness and Gel Film to Ceramic Film Conversion. *J. Am. Ceram. Soc.* **2002**, *85*, 2696.
(38) Zheng, J.; Tan, G.; Shan, P.; Liu, T.; Hu, J.; Feng, T.; Yang, L.; Zhang, M.; Chen, Z.; Lin, Y.; Lu, J.; Neuefeind, J. C.; Ren, Y.; Amine, K.; Wang, L. W.; Xu, K.; Pan, F. Understanding Thermodynamic and Kinetic Contributions in Expanding the Stability Window of Aqueous Electrolytes. *Chem* **2018**, *4*, 2872.
(39) Gobichon, A.-E.; Auffredic, J.-P.; Louër, D. Thermal Decomposition of Neutral and Basic Lanthanum Nitrates Studied with Temperature-Dependent Powder Diffraction and Thermogravimetric Analysis. *Solid State Ionics* **1996**, *93*, 51.
(40) Mentus, S.; Jelić, D.; Grudić, V. Lanthanum Nitrate Decomposition by Both Temperature Programmed Heating and Citrate Gel Combustion: Comparative Study. *J. Therm. Anal. Calorim.* **2007**, *90*, 393.
(41) da Silva, D. G.; Vasconcelos, W. L. Effect of Sol-Gel Processing Parameters on Structure of Zirconia. *Ceramica* **2019**, *65*, 17.
(42) Harvey, E. J.; Whittle, K. R.; Lumpkin, G. R.; Smith, R. I.; Redfern, S. A. T. Solid Solubilities of $(La, Nd)_2$ $(Zr, Ti)_2O_7$ Phases Deduced by Neutron Diffraction. *J. Solid State Chem.* **2005**, *178*, 800.
(43) Brazel, S. W.; Balling, J. R. C. Temporal Analysis of Long-Term Atmospheric Moisture Levels in Phoenix, Arizona. *J. Clim. Appl. Meteorol.* **1986**, *25*, 112.
(44) Abbattista, F.; Vallino, M.; Mazza, D. Preparation and Characterization of $La_2Li_{0.5}Al_{0.5}O_4$ with K_2NiF_4 Structure. *Inorg. Chim. Acta* **1987**, *140*, 147.
(45) Gordon, Z. D.; Yang, T.; Gomes Morgado, G. B.; Chan, C. K. Preparation of Nano- and Microstructured Garnet $Li_7La_3Zr_2O_{12}$Solid Electrolytes for Li-Ion Batteries via Cellulose Templating. *ACS Sustainable Chem. Eng.* **2016**, *4*, 6391.
(46) Xie, H.; Li, Y.; Goodenough, J. B. Low-Temperature Synthesis of $Li_7La_3Zr_2O_{12}$. *Mater. Res. Bull.* **2012**, *47*, 1229.

DOI: 10.1021/acs.iecr.9b03376
Ind. Eng. Chem. Res. 2019, 58, 17399−17405